J. Fluid Mech. (1983), *vol.* 127, *pp.* 473–496
Printed in Great Britain

Experimental and theoretical investigation of backward-facing step flow

By B. F. ARMALY†, F. DURST‡, J. C. F. PEREIRA AND B. SCHÖNUNG

Institute of Hydromechanics, Section III: Mechanics of Turbulent Flows, University of Karlsruhe, Kaiserstraße 12, D-7500 Karlsruhe, F.R.G.

(Received 5 August 1980 and in revised form 26 July 1982)

Laser-Doppler measurements of velocity distribution and reattachment length are reported downstream of a single backward-facing step mounted in a two-dimensional channel. Results are presented for laminar, transitional and turbulent flow of air in a Reynolds-number range of $70 < Re < 8000$. The experimental results show that the various flow regimes are characterized by typical variations of the separation length with Reynolds number. The reported laser-Doppler measurements do not only yield the expected primary zone of recirculating flow attached to the backward-facing step but also show additional regions of flow separation downstream of the step and on both sides of the channel test section. These additional separation regions have not been previously reported in the literature.

Although the high aspect ratio of the test section (1:36) ensured that the oncoming flow was fully developed and two-dimensional, the experiments showed that the flow downstream of the step only remained two-dimensional at low and high Reynolds numbers.

The present study also included numerical predictions of backward-facing step flow. The two-dimensional steady differential equations for conservation of mass and momentum were solved. Results are reported and are compared with experiments for those Reynolds numbers for which the flow maintained its two-dimensionality in the experiments. Under these circumstances, good agreement between experimental and numerical results is obtained.

1. Introduction

The phenomena of flow separation of internal flows caused by sudden changes in test-section geometries is well known. The importance of such flows to engineering equipment has been stressed in many publications (e.g. see Abbot & Kline 1962; Seban 1964; Goldstein *et al.* 1970), and attempts have been made to develop advanced experimental and theoretical techniques in order to study carefully flows with separation regions (e.g. see Durst & Whitelaw 1971; Gosman & Pun 1974; Kumar & Yajnik 1980). However, it is only recently that these techniques have reached the required state of development so that they can be of immediate use in fluid-mechanical studies of internal flows with regions of recirculation. In the past, most experimental studies relied on flow-visualization techniques and/or heat- and mass-transfer

† Present address: Mechanical Engineering Department, University of Missouri–Rolla, Rolla, Missouri 65401, U.S.A.

‡ Present address: Lehrstuhl für Strömungslehre, Universität Erlangen–Nürnberg, Egerlandstraße 13, D-8520 Erlangen, F.R.G.

measurements to obtain fluid-mechanical information in separated flows. Although the obtainable information was limited to what one might call integral flow parameters, several publications have become available for various flow geometries. Among these, the two-dimensional backward-facing step has received particular attention owing to its geometrical simplicity (e.g. see Denham & Patrick 1974; Etheridge & Kemp 1978; Wauschkuhn & Vasanta Ram 1975*a*, *b*). Relying on information for boundary-layer flow behaviour, it was believed that this simple flow geometry should also yield a simple flow pattern showing a single separation region attached to the step, as sketched in figure 1. In most of the available work the length of the separation region was thought to be only dependent on the Reynolds number, on the step height and on the momentum thickness of the oncoming flow (e.g. Etheridge & Kemp 1978; Wauschkuhn & Vasantaram 1975*a*, *b*). The results were thought to scale with the dimensions of the recirculation region attached to the step (e.g. see Gersten & Wauschkuhn 1978; Eaton & Johnstone 1980), and other regions of detached flow were not measured and/or have not been reported so far. Most of the existing work also concentrates on laminar and turbulent flows only, leaving out the region of transitional flows. In addition, very few data exist for laminar and turbulent flows in the same test-section geometry, and hence very little is known on the variation of flow structure with Reynolds number without any changes in test-section geometry.

The present research work was carried out to add to the existing knowledge of backward-facing step flow and to deepen the understanding of internal flow with separation by measurements of velocity distributions over a wide Reynolds-number range covering laminar, transitional and turbulent flows. A laser-Doppler anemometer was employed to define quantitatively the variation of separation length with Reynolds number and to obtain detailed information on the velocity proflies downstream of the step. The experimental results show mutiple regions of separation downstream of the backward-facing step on both sides of the channel walls. Such regions will strongly influence heat and mass transfer, as shown by Kottke, Blenke & Schmidt (1977), Sparrow & Kaljes (1977) and Armaly, Durst & Kottke (1980). Understanding the details of internal flows with multiple regions of separation will also help to deepen the insight into heat and mass transfer associated with them.

The present experimental study yielded two-dimensional flows only at Reynolds numbers $Re < 400$ and $Re > 6000$. In between these Reynolds numbers the flow was found to be strongly three-dimensional, but always maintained its symmetry to the centreplane of the test section. This fact is clearly documented in this paper, providing an insight into the complex structure of the flow.

Two-dimensional numerical predictions of mean-velocity distributions of backward-facing step flow were also carried out by the authors, and examples of predictions are presented in this paper. Good agreement is obtained between experimental and theoretical results for Reynolds numbers smaller than 400, where the required two-dimensionality of the flow could be maintained. Although numerical prediction procedures encounter false diffusion, the good agreement between the predicted and measured flow field for $Re < 400$ demonstrates that truncation errors due to 'false diffusion' could be kept very low. For Reynolds numbers larger than 400, two-dimensional predictions were also obtained, and results are provided that also show multiple regions of recirculating flow. The longitudinal extensions of these regions are given in diagrams and are compared with those obtained experimentally. Some of the differences are explained as being caused by the three-dimensionality of the flow. These conclusions are supported by additional information drawn from heat- and mass-transfer measurements carried out in the same test section.

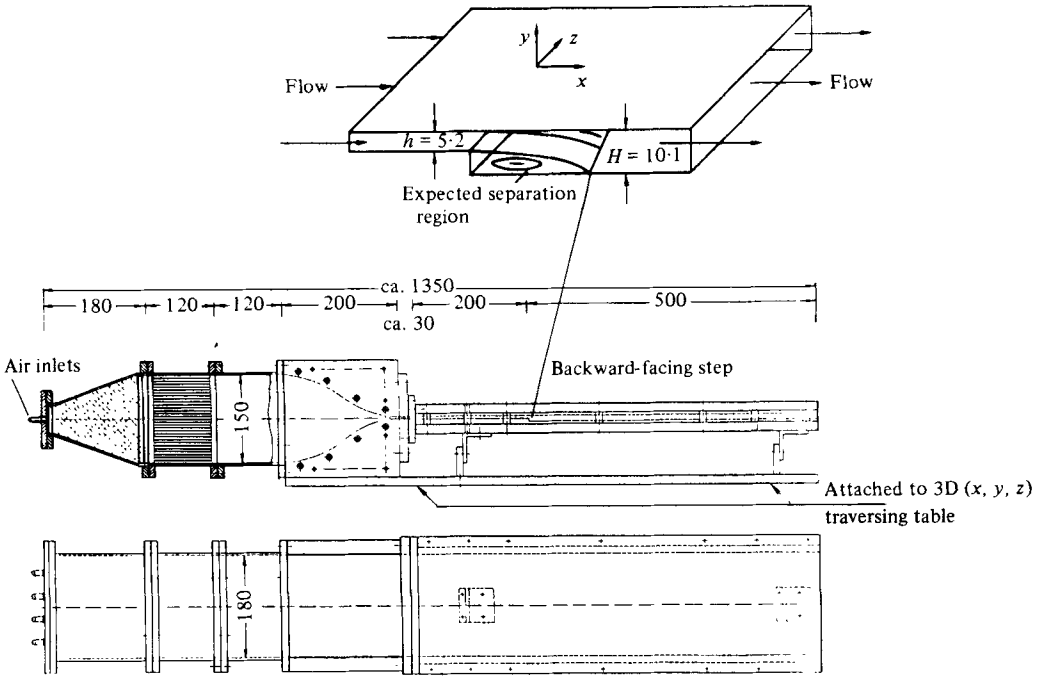

FIGURE 1. Schematic of air tunnel and test section (dimensions in mm).

2. Experimental investigation

2.1. *Apparatus and experimental procedures*

The open air-driven flow channel that was used for this study is shown schematically in figure 1. It incorporated a two-dimensional backward-facing step that provided an expansion ratio of 1 : 1·94. The larger channel, downstream of this step, had a height of 1·01 cm and an aspect ratio of 18 : 1. The tunnel and the test section were constructed from aluminium and all parts were machined to very close tolerances regarding parallelity of walls, surface roughness, manufacturing of step corners, etc. The two sidewalls were made of glass of 1 cm thickness to support the rigidity of the test section and also to facilitate laser-Doppler measurement with forward-scattered light. The air flow into the channel contained scattering particles of 2 μm mean diameter provided by a silicone-oil particle generator described by Cherdron, Durst & Whitelaw (1978). The air flow with particles was passed through a large settling chamber and was fed through five, 6 mm diameter, bored tubes into the first part of the flow channel. This part consisted of an expansion section packed with steel wool to smoothen the flow and to prevent input disturbances from affecting the measurements. The flow was then passed through a section with flow straighteners and was afterwards guided into a smooth contracting nozzle with an inlet-to-outlet area ratio of 30 : 1. The outlet of the nozzle was connected to the inlet of the channel test section, which was 0·52 cm in height and 20 cm in length up to the backward-facing step. These dimensions ensured a two-dimensional fully developed flow at the cross-section where the step was located for the entire Reynolds-number range studied by the authors. The upper and the lower part of the test section and the glass sidewalls were held parallel together by machine screws and were attached to the nozzle exit by location pins. The assembly of channel and inlet section was placed on the top of a three-dimensional traversing table which allowed the measuring

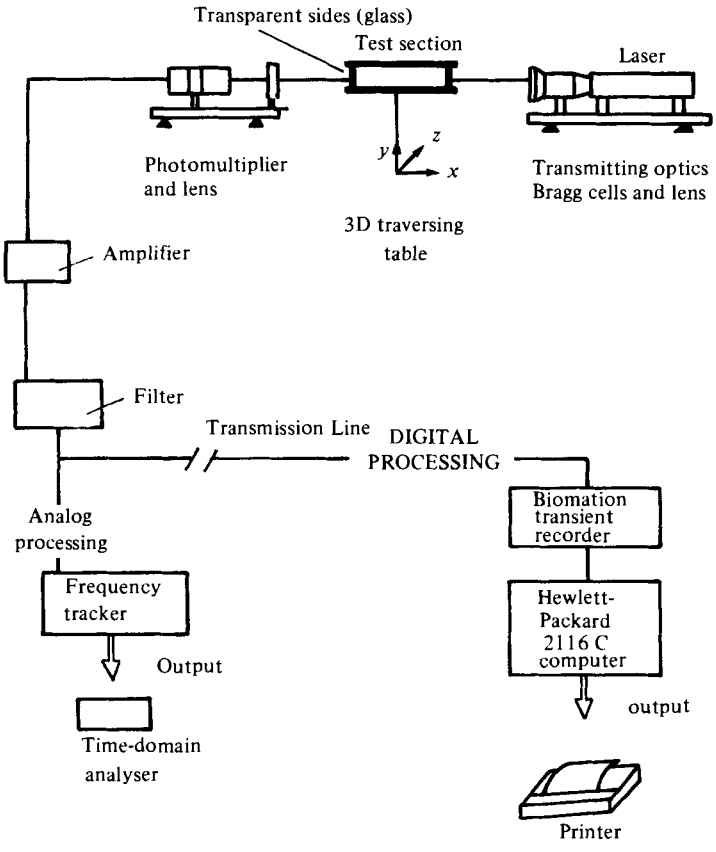

FIGURE 2. Block diagram of data acquisition and processing system for LDA measurements.

position to be located to within 0·1 mm in the x- and z-directions and to within 0·01 mm in the y-direction. This coordinate system is indicated in figure 1 together with the dimensions of the test section and some details of the construction.

The laser-Doppler anemometer used in the experiments was operated in the so-called fringe mode, with an optical arrangement similar to that used by Cherdron *et al.* (1978). It was employed in the forward-scattering mode and was set up to measure only the x-velocity component, that is, parallel to the channel walls and along the channel axis. The optical system consisted of a 15 mW He–Ne laser, integrated, although modular, transmission optics with Bragg cells, light-collecting optics with photomultiplier, and the signal-processing equipment corresponding to the block diagram of figure 2. Two frequency-tracking demodulators (BBC-Goertz LS301 and Cambridge Consultants CC04) were initially used to process the Doppler signals. These two trackers proved to be incapable of properly tracking the Doppler signals in the neighbourhood of the reattachment zone for Reynolds numbers larger than 2000. This was due to the high turbulence levels and the low particle rate in that region, as well as the observed deterioration of signal quality very near to the wall. For that reason, a Biomation transient recorder was used to digitize and store the signals from the photomultiplier. The stored signals were transferred to a Hewlett–Packard Computer (HP 2116) and processed to yield the required Doppler frequency of individual bursts. Time-averaged velocities and turbulence intensities were computed from these individual Doppler frequencies. All the results presented in this paper were processed

with the signal-processing system based on the transient recorder and computer. This is discussed in more detail in a report by Durst & Tropea (1977).

In order to obtain information on velocity profiles, the optical system was spatially fixed and the test section was moved in steps, with the abovementioned three-dimensional traversing table to record the velocity information at fixed positions in space.

The velocity profile $U(x = 0, y)$ at the step was close to a parabolic profile, but showed systematically small deviations due to the pressure gradient enforced by the step. The inlet profile was carefully recorded for all Reynolds numbers. Flow rates were varied by adjusting the regulating valves available in the air supply. For each flow rate, the silicone-oil particle rate was also adjusted to insure a sufficiently high particle concentration for each flow rate to permit proper processing of the Doppler signals, e.g. to provide individual Doppler bursts at a signal rate yielded approximately 100 signal bursts per second.

To measure the reattachment length at a given flow rate, the inlet velocity was measured to determine the Reynolds number, and then the lower and the upper walls were scanned in the x-direction and at constant and known y-position. To determine the reattachment length of the primary separation region and the locations of detachment and reattachment of additional regions of recirculating flow behind the step, the position of the zero-mean-velocity line was measured. The points of detachment and reattachment were taken as the extrapolated zero-velocity line down the wall, e.g. x_R is determined from the following relationship:

$$x = x_0(y_0): \lim_{T \to \infty} \frac{1}{T} \int_0^T U(x_0(y_0), y_0, t)\, dt = 0,$$

$$\lim_{y_0 \to 0} x_0(y_0) = x_R.$$

For a given measurement of local time-mean velocity at a known (x, y) position, 100–5000† Doppler bursts, with each having at least 20 signal cycles, were processed and averaged. The Biomation transient recorder was externally triggered at a rate much slower than the occurring Doppler bursts to eliminate biasing for time-varying flow conditions. A time of 1–5 minutes, depending on the state of the flow and the location in the flow field, was needed for each measuring point to gather and process the required number of Doppler bursts. The location of the measuring point was determined from the dial readings of a traverse table with the zero locations being $x = 0$ at the step and $y = 0$ at the test-section wall where the step is located, and $z = 0$ being the centreplane of the channel test section. The cross-sectional velocity profiles $U(y)$ at fixed x- and z-locations were measured by prechoosing the x- and z-locations and by varying the y-position in predetermined steps. The mean Doppler frequency of 100–5000 Doppler bursts was determined for each measuring position, and the mean longitudinal velocity component computed according to

$$\bar{U}(x,y,z) = \frac{\bar{f}_D \lambda}{2 \sin \phi} = \frac{\lambda}{2 \sin \phi} \lim_{T \to \infty} \frac{1}{T} \int_0^T f_D(x,y,z,t)\, dt,$$

where f_D is the instantaneous Doppler frequency, λ the wavelength of the employed laser radiation, and ϕ the half-angle between the two laser beams being crossed inside the measuring control volume.

† The number was dependent on the state of the flow (laminar or turbulent) and on the local turbulence intensity.

2.2. *Experimental results*

2.2.1. *Longitudinal flow structure.* Measurements of the reattachment length and velocity distribution were performed for a Reynolds-number range between 70 and 8000, which covered the laminar, transitional and part of the turbulent regime of the two-dimensional backward-facing step flow. The definition of the Reynolds number which is used in this study is given by

$$Re = \frac{VD}{\nu},$$

where V is two-thirds of the measured maximum inlet velocity, which corresponds in the laminar case to the average inlet velocity, D is the hydraulic diameter of the inlet (small) channel and is equivalent to twice its height, $D = 2h$, and ν is the kinematic viscosity. In all of the cases that are reported here the average velocity was determined from measurements of velocity at the centre of the inlet channel at about 1 cm upstream of the step. Reynolds numbers used in step-flow studies such as the one based on centre velocity and/or step height can be easily deduced from the stated definition and from the 'inlet' mean-velocity profile measurement for each Reynolds number.

The attempted two-dimensionality of the flow in the inlet channel was confirmed by measurements. The flow in the plane of the sudden expansion in the inlet channel was symmetric and two-dimensional over the centre 150 mm of its width to within 1 %, as shown in figure 3. In the laminar range, the velocity field was close to that of a fully developed channel flow with a slight deviation from a parabolic profile. This was caused by the pressure change downstream of the sudden expansion. The section length downstream of the step was sufficiently long to permit the flow to redevelop into a fully developed channel flow, i.e. $\partial U/\partial x = 0$. As expected, with increasing Reynolds number, the length of flow development downstream of the step increased. At the outlet of the test section, a fully parabolic profile was established for the small Reynolds numbers, but small deviations were present for the higher ones.

Measurements of reattachment length x_1 are shown in figure 4 as a function of Reynolds number. From the shape of this curve one can clearly identify the laminar ($Re < 1200$), the transitional ($1200 < Re < 6600$) and the turbulent ($Re > 6600$) regimes of the flow. To the authors' knowledge this is the first detailed measurement, via a laser-Doppler anemometer, of reattachment-length variation with Reynolds number that covers the three different regimes of flow and defines them on the basis of actual velocity measurements. Previous studies of this property have been carried out by means of flow-visualization techniques or were performed on the basis of heat- and mass-transfer measurements (e.g. see Back & Roschke 1972; Filetti & Kays 1967; Sparrow & Kaljes 1977; Kottke *et al.* 1977). The laminar regime of the flow is characterized by a reattachment length that increases with Reynolds number. The increase is, however, not linear as suggested for reattachment-length variations in axisymmetric sudden pipe expansions (see Macagno & Hung 1967). This fact has also been demonstrated by Denham & Patrick (1974), who reported on a laminar-flow study in a geometry similar to the present one but with an expansion ratio of 3:2. However, they had velocity profiles at the step that strongly deviated from the laminar nearly parabolic profile set up in the present case.

The regime of transitional flow ($1200 < Re < 6600$) is characterized by first a sharp decrease in the reattachment length x_1, a continued gradual, but irregular decrease to a minimum value at a Reynolds number of approximately 5500, then an increase

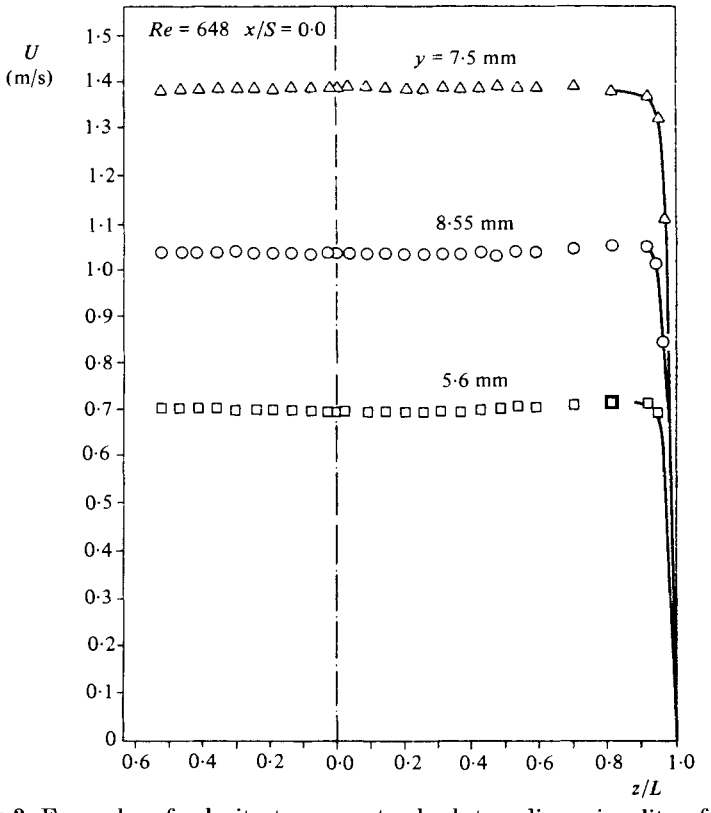

FIGURE 3. Examples of velocity traverses to check two-dimensionality of the inlet flow.

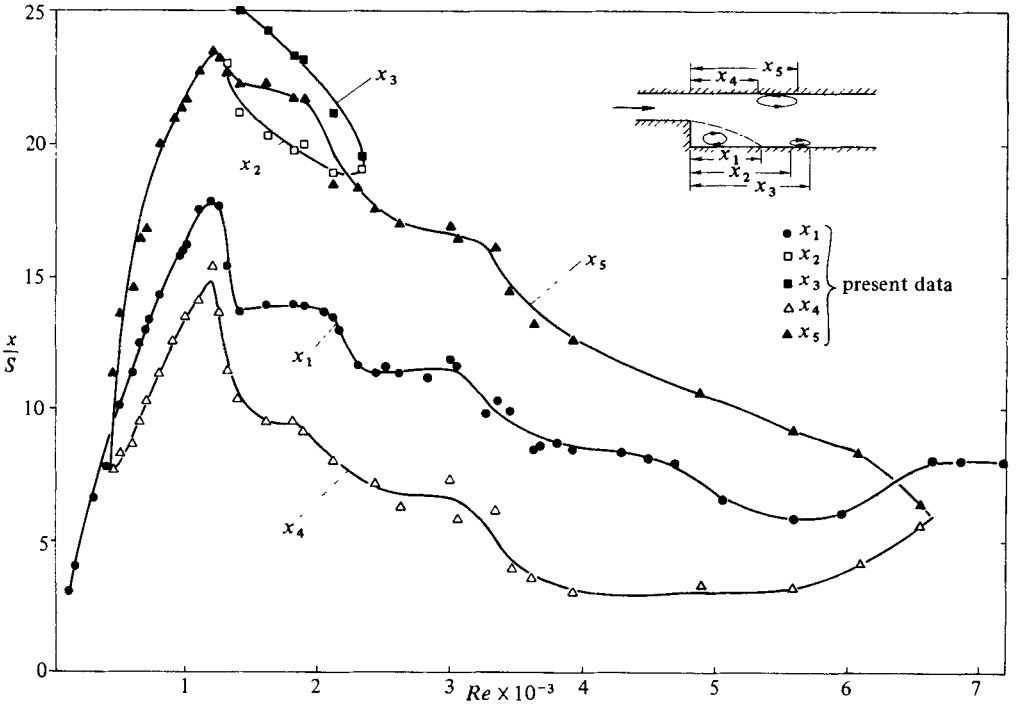

FIGURE 4. Location of detachment and reattachment of the flow at the centre of the test section; variation of locations with Reynolds number.

to a constant level that characterizes the turbulent-flow regime. An additional recirculating-flow region was measured downstream of the primary region of separation, and its extension is shown in figure 4 as x_2 and x_3. This additional region of circulating flow has not been previously reported in the literature. It is very thin, approximately 0·4 mm, with an x-extension given in figure 4. It originates in the Reynolds-number range corresponding to the early part of the transition region (see figure 4), where the reattachment length experiences a sharp drop in its magnitude. Cherdron *et al.* (1978) and Sparrow & Kaljes (1977) believed these strong variations in flow properties to be caused by vortex shedding from the edge of the step. These vortices were thought to approach the wall, and the second region of recirculating flow might then be due to the sharp change of flow direction which the eddies experience. Figure 4 shows that the length of this secondary recirculation region decreases rapidly with Reynolds number, and it disappears for Reynolds numbers larger than 2300. Such a second separation bubble might have been the cause of the second maximum observed by Sparrow & Kaljes (1977) in their mass-transfer measurements.

The turbulent range ($Re > 6600$) is characterized by a constant reattachment length. The measured value in that region is in agreement with the one measured by Abbot & Kline (1962) in a similar test-section geometry at higher Reynolds numbers. It is interesting to note that in the turbulent region de Brederode & Bradshaw (1972) for $H/h = 1{\cdot}2$ measured $X_R/S = 6$, also Moss, Baker & Bradbury (1979) for $H/h = 1{\cdot}1$ measured $X_R/S = 5{\cdot}5$. These data suggest that, as the expansion ratio H/h decreases, a lower reattachment-length to step-height ratio X_R/S is obtained. This is confirmed by the detailed measurements of Durst & Tropea (1981), who studied the dependence of the reattachment length of the primary separation region as a function of Reynolds number and expansion ratio, but only in the larger-Reynolds number range.

An additional recirculating-flow region was measured at the upper wall downstream of the expansion, as shown in figure 4. To the authors' knowledge, this separation region has also not been previously reported in the literature. It develops in the laminar range and remains in existence throughout the transition region. Its appearance is due to the adverse pressure gradient created by the sudden expansion, and its existence is largely dependent on the expansion ratio of the backward-facing-step flow geometry. As figure 4 shows, this separated-flow region exists for Reynolds numbers higher than approximately 400, and it disappears in the Reynolds-number range that corresponds to the end of the transitional-flow regime. Figure 4 shows the longitudinal extension of the third region of separated flow which existed in parts of the laminar flow regime and the regime of laminar–turbulent transition. The results indicate that the length of this separated-flow region initially increases with Reynolds number and thereafter decreases and disappears above a Reynolds number of approximately $Re > 6600$.

Figure 4 summarizes the locations of the three circulation regions. It clearly demonstrates that, for most of the investigated Reynolds-number range, the beginning of the recirculation region at the upper wall is upstream from the reattachment point of the primary recirculating flow region and its end is downstream from it. Detailed measurements of the velocity profile in this flow geometry at different x-positions are presented in figures 5 and 6 for Reynolds numbers 1095 and 1290 respectively. Further measurements are provided in §3 together with flow computations. All extensive velocity measurements carried out by the authors were of the x-velocity component U, and were taken at the centreplane of the channel, $z = 0$, where the flow was expected to be two-dimensional. The measurements demonstrated

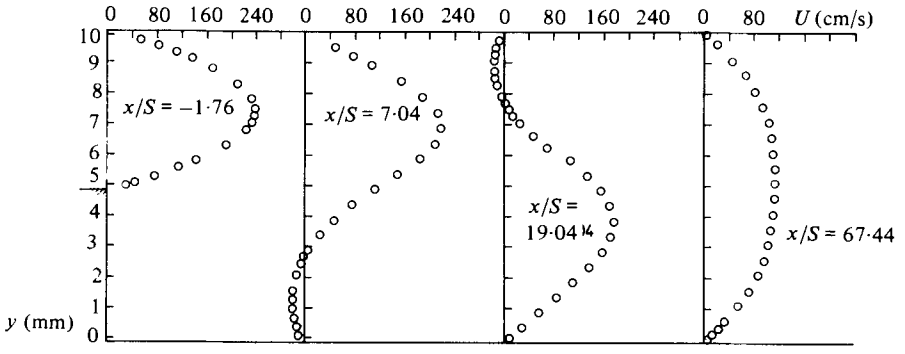

FIGURE 5. Velocity profiles for $Re = 1095$.

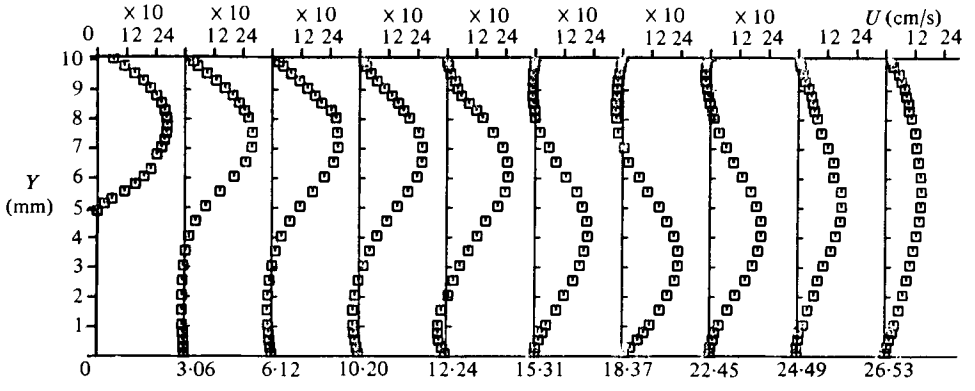

FIGURE 6. Velocity profiles for $Re = 1290$.

that in the laminar range the velocity profile before before the step, e.g. at $X/S = -4$, was parabolic, and only a small deviation from that profile was measured at the step, $X/S = 0$. The velocity profiles indicate that the flow separated at the step, resulting in one, two or three recirculation regions behind the step, and then redeveloped to a fully developed parabolic velocity profile in the larger channel. A velocity scan at a distance of 0·6 mm away from the upper wall is presented in figure 7 for a Reynolds number of 1095 to demonstrate more clearly the occurrence of the recirculating flow region at the wall opposite to the step. Along that plane 0·6 mm away from the upper wall the velocity decreases with distance away from the step, and it becomes negative at $X = 76$ mm. At $X = 120$ mm the region of negative velocity ends and positive velocity occurs again beyond that point. The thickness of this recirculation region for that Reynolds number and at $X/S = 19{\cdot}04$ can be seen in figure 5 to be 0·22 cm.

Similar results were also obtained for Reynolds numbers in the transitional-flow regimes where both secondary separation regions existed. These measurements indicated that, in the transitional-flow regime, the recirculating-flow region on the upper wall moves upstream as the Reynolds number increases, and the shape of the velocity profile within it is skewed towards the downstream end. In the Reynolds-number range $1200 < Re < 2300$ the second recirculating-flow region on the lower wall exists, as seen from figure 4. It occupies a relatively small volume and the velocities within it are small.

2.2.2. *Spanwise flow structure.* The present experimental investigations were carried out for inlet and outlet conditions set up to yield nominally two-dimensional

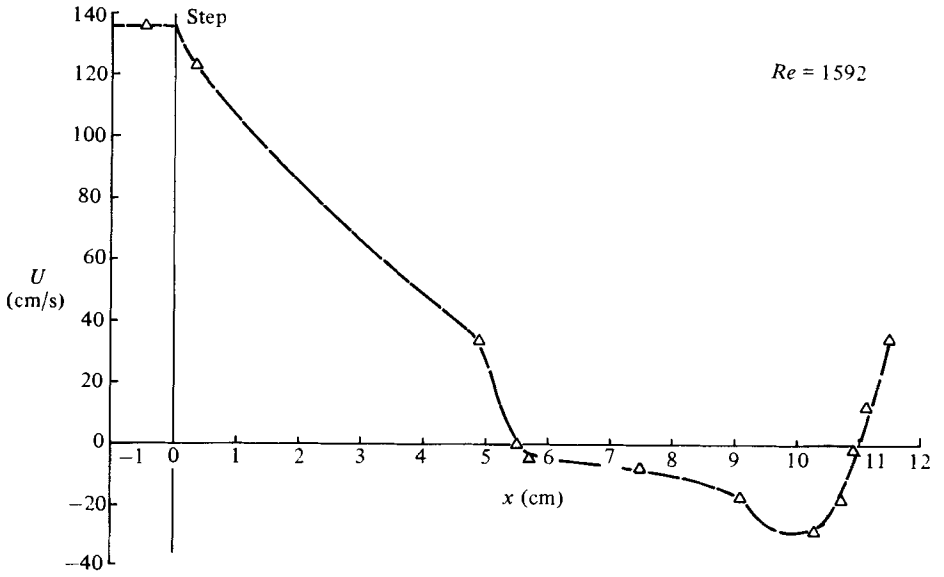

FIGURE 7. Scan of upper wall at a wall distance of 0·6 mm and $Re = 1592$.

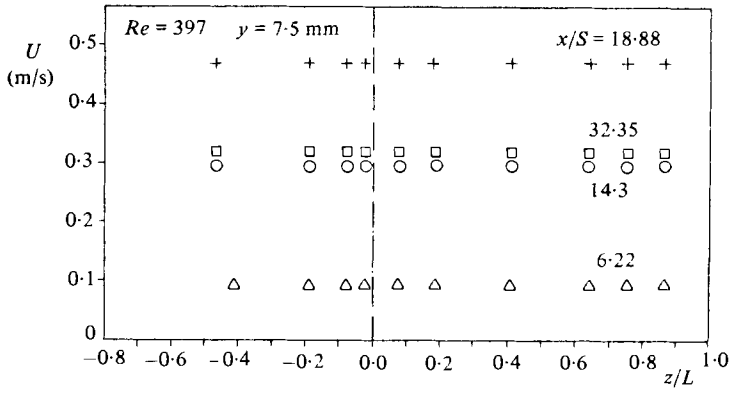

FIGURE 8. Example of mean-velocity profiles to demonstrate the two-dimensionality of the flow for $Re = 397$.

flow at the step location and very far downstream of the step. Irrespective of this, the flow downstream, in the immediate vicinity of the step, was found to be three-dimensional within the Reynolds-number range $400 < Re < 6600$. At Reynolds numbers smaller than 400 the flow maintained its two-dimensionality, as indicated in figure 8 for a Reynolds number $Re = 397$. This figure gives spanwise velocity profiles at various x-locations and at a fixed y-position and shows the constant velocity values obtained for various z-locations. The two-dimensionality of the flow for this Reynolds number is also demonstrated by the spanwise location of the reattachment line shown in figure 9. The same figure also provides the location of the reattachment line for the primary separated-flow region for a Reynolds number $Re = 648$, and indicates the three-dimensionality of the flow at Reynolds numbers in the range where multiple regions of separated flow occur. For $Re = 648$ more details of the spanwise flow structure are obtained from figures 10(a, b), providing examples of measured spanwise velocity profiles at various x-locations and for two fixed

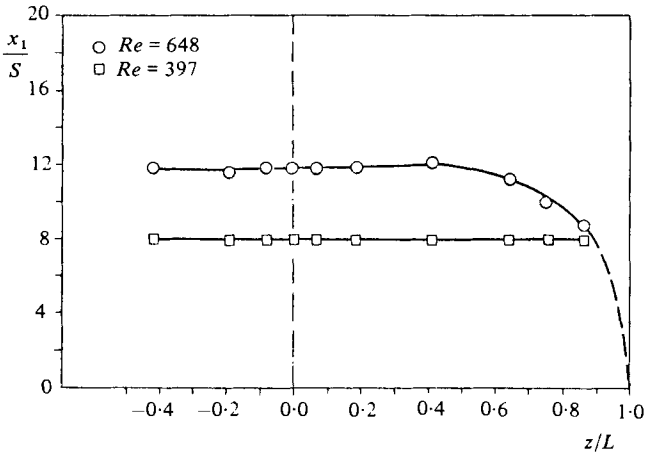

FIGURE 9. Spanwise location of reattachment line for two Reynolds numbers.

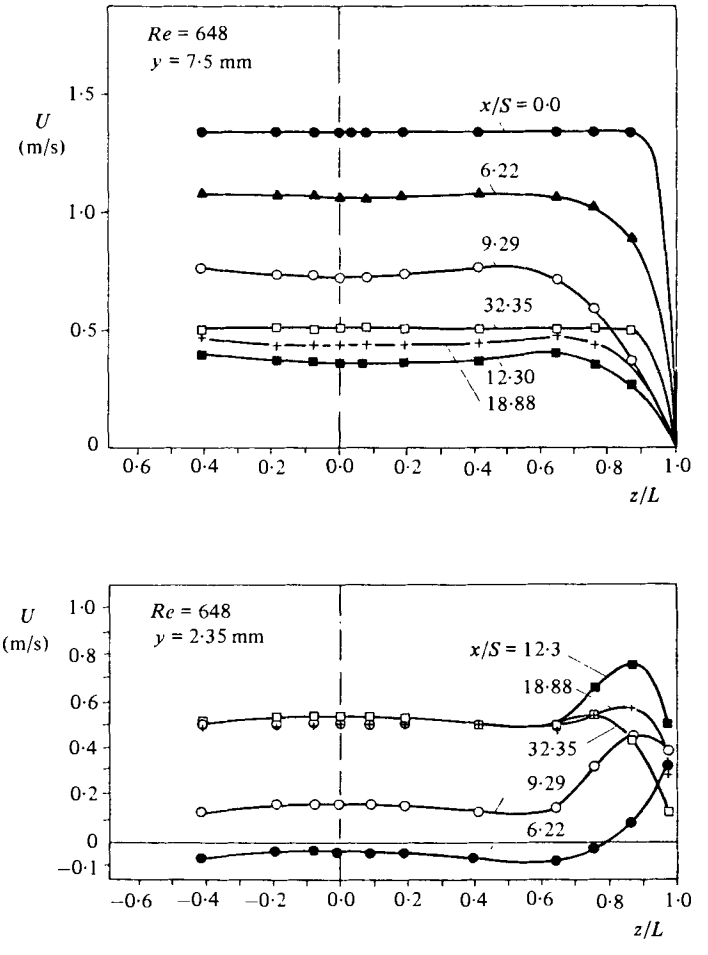

FIGURE 10. Examples of spanwise mean velocity profiles to demonstrate three-dimensionality of the flow.

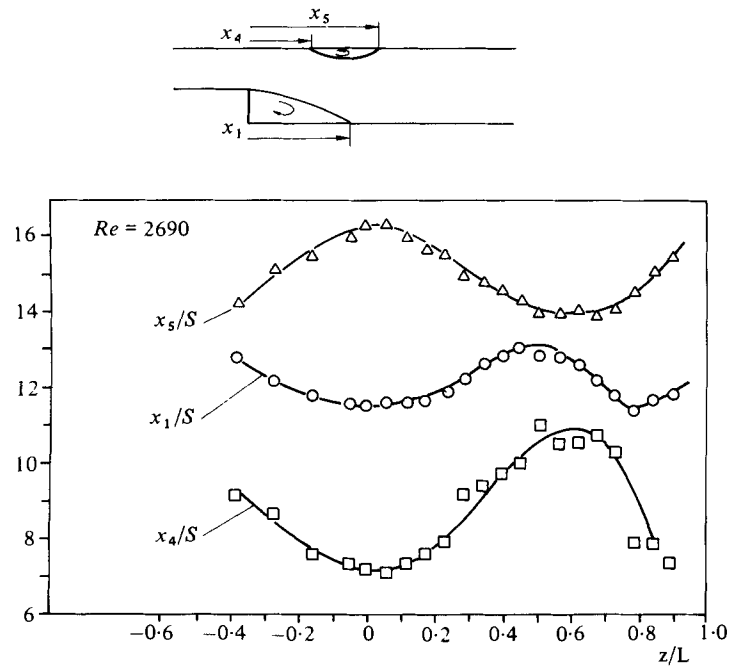

FIGURE 11. Variation of spanwise location of line of detachment and reattachment for $Re = 2690$.

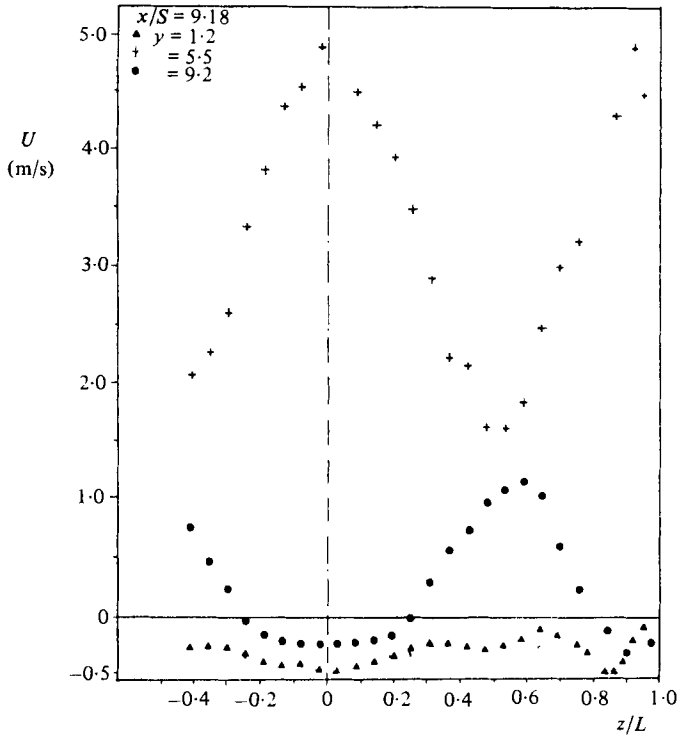

FIGURE 12 (part). For caption see facing page.

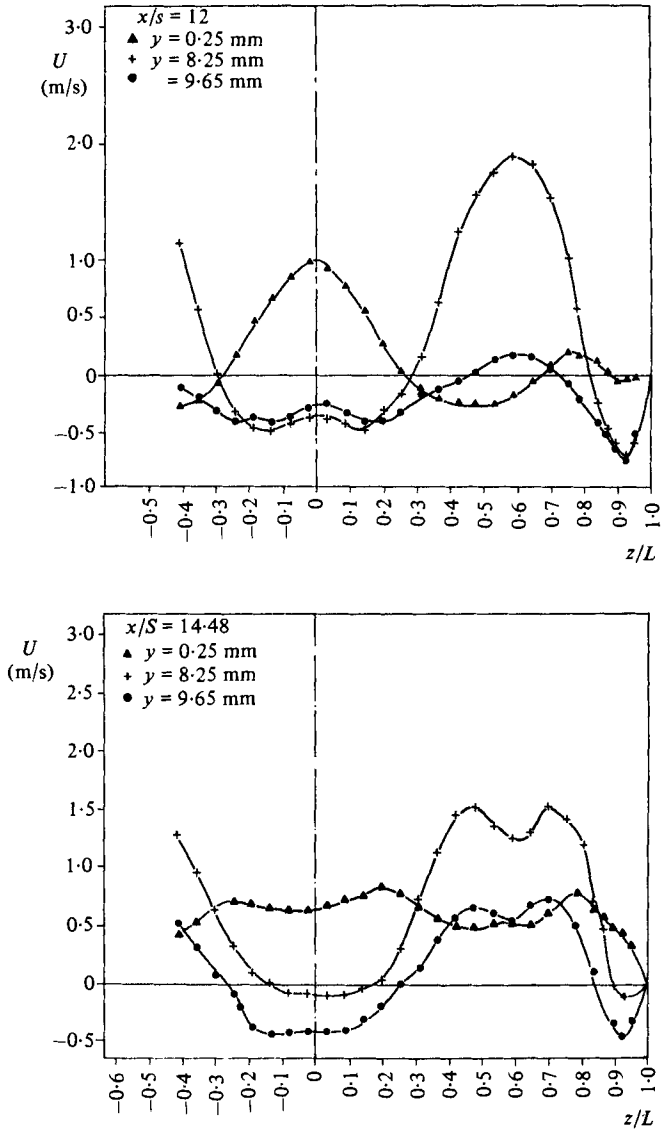

FIGURE 12. Spanwise velocity profiles for various x- and y-locations for $Re = 2690$.

y-positions. These clearly indicate the three-dimensionality of the flow for Reynolds numbers in excess of approximately 400.

The three-dimensionality of the flow indicated in figure 10 is enhanced with increasing Reynolds number. This was quantified by detailed velocity measurements for various Reynolds numbers, and figures 11 and 12 show a data set for a Reynolds number $Re = 2690$. The spanwise locations of the lines of separation and reattachment are shown in figure 11 and indicate that the longitudinal extensions of the recirculating-flow regions vary across the test-section width. Whenever the longitudinal extension of the separation region opposite to the step increases, the primary region of separated flow attached to the step decreases and *vice versa*. The extensions of both recirculating-flow regions are strongly coupled, as can be seen from figure 11.

Figure 11 clearly demonstrates the three-dimensionality of the flow, and this is further supported by the spanwise velocity profiles provided in figures 12(*a–c*). The momentum of the main flow 'deforms' the dividing streamline of the upper separated-flow region, yielding streaklike flow patterns in the direction of the flow and located across the channel test section. It is worth noting that the flow maintains its two-dimensionality up to x-positions where the separation region opposite to the step starts. The two-dimensionality of the flow is again re-established at $x/s \approx 19$. Between these x-locations the flow is strongly three-dimensional.

3. Theoretical investigations

3.1. *Governing equations and solution procedure*

Predictions of the laminar flow field in a geometry equivalent to the case used for the experiments were obtained by numerically solving the governing elliptic differential equations. The flow was considered to be two-dimensional and stationary. The governing equations are as follows:

continuity equation

$$\frac{\partial}{\partial x}(\rho U)+\frac{\partial}{\partial y}(\rho V)=0;$$

momentum equations

$$\frac{\partial}{\partial x}(\rho U^2)+\frac{\partial}{\partial y}(\rho UV)=-\frac{\partial p}{\partial x}+\mu\left(\frac{\partial^2 U}{\partial x^2}+\frac{\partial^2 U}{\partial y^2}\right),$$

$$\frac{\partial}{\partial x}(\rho UV)+\frac{\partial}{\partial y}(\rho V^2)=-\frac{\partial p}{\partial y}+\mu\left(\frac{\partial^2 V}{\partial x^2}+\frac{\partial^2 V}{\partial y^2}\right);$$

where U, V are the velocities in the (x, y)-coordinate directions, ρ is the density, μ is the dynamic viscosity and p is the pressure. The boundary conditions applied for the computations were as follows:

$$\text{walls:}\quad U=V=0;$$

$$\text{inlet:}\quad U=\text{measured},\quad V=0;$$

$$\text{exit at } x=l:\quad \frac{\partial U}{\partial x}=0,\quad \frac{\partial V}{\partial x}=0.$$

The length L measured from the step to the end of the calculation domain was selected to be equivalent to at least four times the experimentally measured reattachment length of the primary recirculation region, $L = 4X_R$, and the boundary condition at that cross-section was taken as that of a fully developed flow, e.g. $\partial U/\partial x = 0$, $\partial V/\partial x = 0$. The chosen distance L has been shown to be sufficient to make the reattachment length independent of the length of the calculation domain.

The solution of the above partial differential equation was obtained by using a finite-difference numerical scheme, embodied in the computer code TEACH (see Gosman & Pun 1974). The solution procedure starts by supplying initial guesses of the velocity and pressure fields and then computes a converged solution by iteration. Convergence of the solution was considered satisfactory when the normalized residuals of each equation, summed over the whole calculation domain, were smaller than 10^{-4}.

The grid distribution in the calculation domain was non-uniform in both the longitudinal and the cross-flow coordinate directions. A large number of grid points were placed in the areas where steep variation in velocities were expected. This information was deduced from experiments and also from preliminary calculations using equally spaced numerical grids. Solutions were performed with different grid densities, and the resulting reattachment length of the primary separated-flow region was studied as a function of grid number. The required grid number to ensure grid independence increased with Reynolds number. It was found that a grid density of $N_x \times N_y = 45 \times 45$ is sufficient to provide a primary reattachment length that is independent of the grid density up to Reynolds number of 400. Based on this, all the numerical results presented in this study up to Reynolds numbers of $Re = 400$ were obtained with a grid density of $N_x \times N_y = 45 \times 45$. For a Reynolds number of 100, a solution utilizing a grid density of 45×45 requires 400 iterations for convergence. The number of iterations increased strongly with Reynolds number up to values where the additional recirculation zones occur. For $Re = 450$ the required number of iterations was 1200, using the same grid density. This required 75 min of computing time on the UNIVAC 1108 of the University of Karlsruhe.

As already mentioned, the two-dimensional flow predictions also yielded multiple regions of separated flow. In order to compute the flow inside these regions accurately, the grid distribution would require further refinements, i.e. more grid points would be needed inside the computational domain, especially in the region where the additional separated-flow regions occur. However, the available UNIVAC 1108 computer did not permit enough grid points for grid independence to be obtained, and hence, with the occurrence of more than one region of separated flow, complete grid independence could not be achieved even with the highest-possible grid number of 2600. This should be borne in mind for assessing fully the validity of the numerical results in §3.2.

3.2. *Numerical results*

Employing the computer code TEACH, flow predictions were carried out to deepen insight into the flow structure of two-dimensional backward-facing step flow. These predictions were performed up to Reynolds numbers $Re = 1250$, at which the flow was found experimentally to turn from the laminar- into the transitional-flow regime. The predicted flow was two-dimensional but still showed multiple regions of separated flow, as can be seen in figures 13(*a*, *b*). These figures show the computed locations of separation and reattachment. They show that the length of the primary separated-flow region is predicted to increase nonlinearly with Reynolds number up to $Re \approx 420$. The ensuing decrease with Reynolds number is caused by the additional region of separated flow that occurs on the wall opposite to the step and at Reynolds numbers larger than $Re > 420$. The longitudinal dimensions of this additional region of separated flow are predicted to increase with Reynolds number up to $Re \approx 980$, above which two more regions of recirculating flow are predicted. Both are located on the channel wall with the step; one inside the primary region of separated flow and the other downstream of its reattachment line. These predicted locations of separated-flow regions are shown in figures 13(*a*, *b*).

Information on the entire flow field was also deduced from the predictions. These confirmed most of the experimental findings about the flow. For smaller Reynolds numbers, the flow shows only the primary region of separated flow attached to the backward-facing step. The additional separated-flow regions occur, however, for the

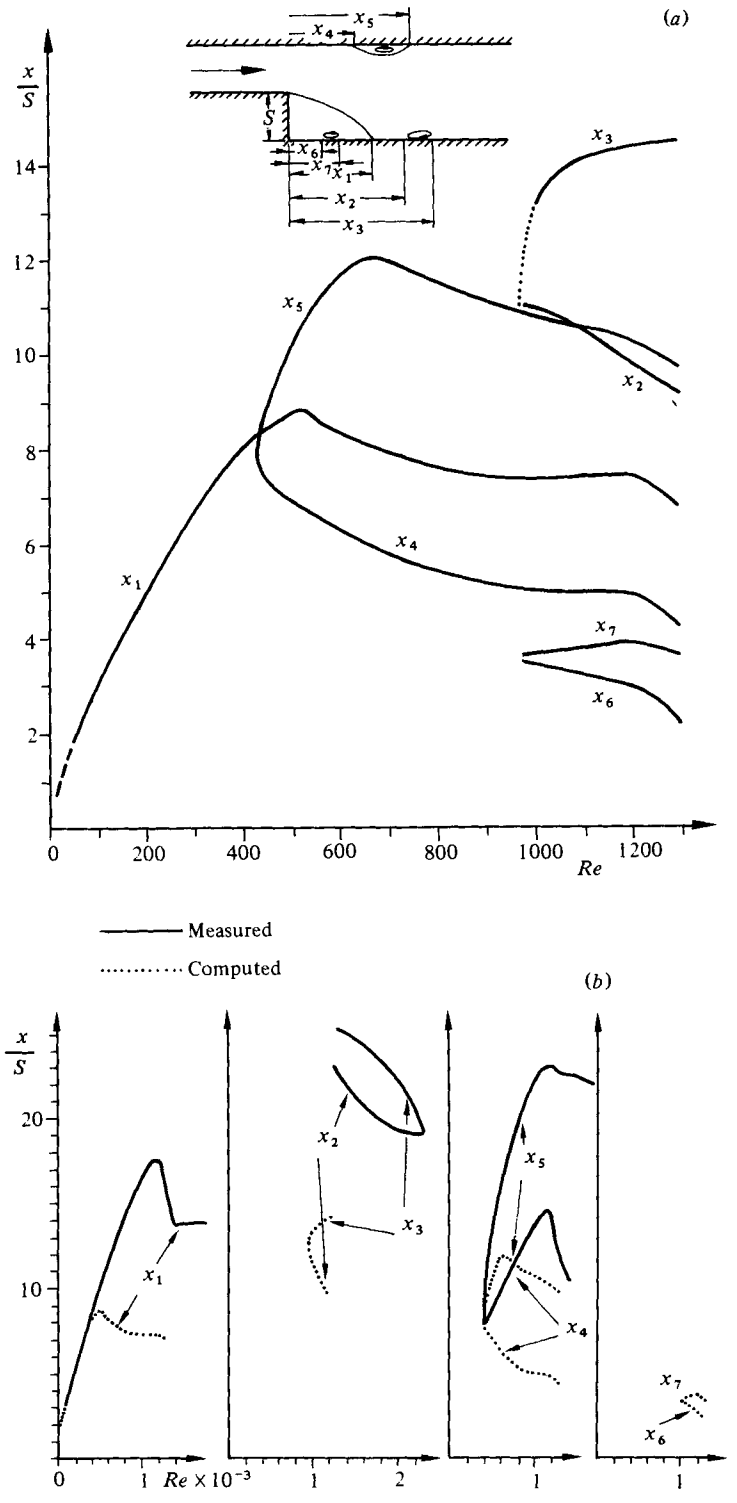

FIGURE 13. (*a*) Predicted location of the flow detachment and reattachment as a function of Reynolds number. (*b*) Comparison of measured and predicted (two-dimensional) locations of detachment and reattachment of the flow.

higher Reynolds numbers. They are located on both sides of the channel walls downstream of the step.

In connection with the accuracy of the flow predictions, some remarks are necessary with respect to the authors' own investigations to establish this accuracy and also with respect to work carried out by other investigators. For all Reynolds numbers studied, the grid Péclet numbers $P_\Phi = \Delta\Phi/\gamma$ for $\Phi = U$ and $\Phi = V$, where Δ is the mesh width and γ the diffusivity, were known from the predictions, as well as the angle that the velocity vector formed at every location with the numerical grid lines. In regions where the velocity vector was strongly inclined to the numerical grid lines and both values of the Péclet number P_Φ were large, grid refinements were introduced in such a way as to decrease the errors due to 'false diffusion' induced by the first-order upwind-difference scheme employed. The redistribution of grid lines emphasized the need to have high-density grids also in regions where strong gradients occurred.

For the Reynolds-number range $Re < 400$ the 'artificial or false diffusion' was negligible, even without satisfying $|P_U| < 2$ in the entire calculation domain. The reason for this is the fact that high Péclet numbers P_U are associated with small angles between the velocity vector and the grid lines.

Two finite-difference schemes were recently developed in order to reduce or eliminate 'false diffusion': the hybrid central skewed-upwind scheme by Raitby (1976) and the quadratic upstream-weighted scheme of Leonard (1979). There have been some comparisons made between these numerical schemes and the hybrid central-upwind-differencing scheme embodied in TEACH (e.g. Castro 1978; Leonard, Leschziner & McGuirk 1978; Leschziner 1980; Leschziner & Rodi 1981). These investigations indicate that the strong storage requirements of the hybrid central-upwind-difference scheme of TEACH can be markedly reduced by these newer schemes, but computational time increases. Additional difficulties in handling higher-order schemes are also worthwhile mentioning.

The comparison carried out by Leschziner (1980) showed that the three different numerical schemes yielded results for backward-facing step flow that were in good agreement with each other. The small differences between the predictions and the experiments of Denham & Patrick (1974) can be explained by the differences in the inlet profiles. Denham & Patrick performed measurements in a channel geometry similar to the present one but having an expansion ratio of 2:3. Last, but not least, it should be mentioned that Castro (1978) and Leschziner (1980) found some disagreement among the three different numerical schemes for the experimental data of Denham & Patrick when comparisons were made at higher Reynolds numbers. This is in general agreement with the present findings.

Because of the above work carried out by the authors to establish the accuracy of their numerical predictions and also owing to similar work available in the literature, other finite-difference schemes than that of the TEACH program were not considered in the present work.

4. Comparison of numerical and experimental results

As explained in §3, converged and grid-independent solutions could be obtained that are in good agreement with experimental findings up to a Reynolds number $Re \approx 400$. For Reynolds numbers in excess of this value the numerical results also show multiple regions of separated (recirculating) flow at the wall opposite to the two-dimensional step and on the channel side where the step is located. Unfortunately,

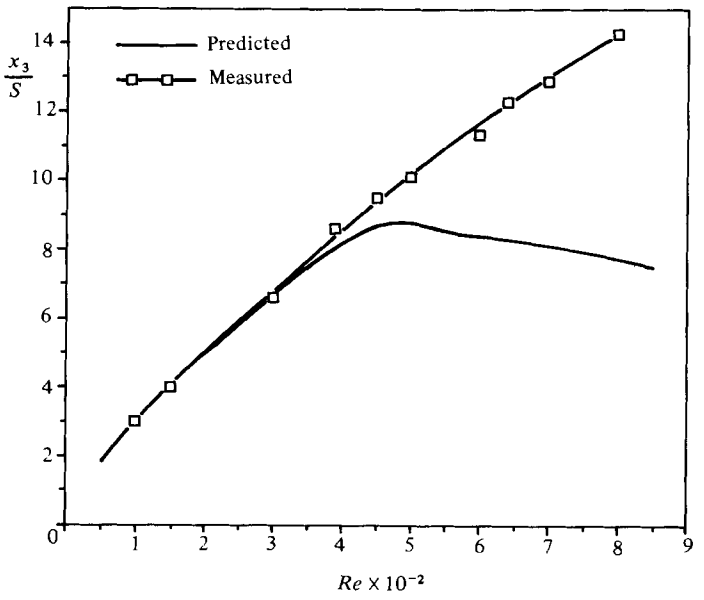

FIGURE 14. Comparison of experimental and theoretical results for the reattachment length up to $Re = 800$.

with the occurrence of more than one separated flow region, the flow in the experiments becomes three-dimensional in the region downstream of the step, and this prevents direct comparison between the experimental and theoretical results. Nevertheless, it is still interesting to make the comparison between the computed and measured separation lengths x_3/S. This information is provided in figure 14.

Figure 15 shows, for a Reynolds number $Re = 100$, comparisons of measured and predicted mean-longitudinal-velocity profiles. These numerical results were obtained for a 45×45 grid for which grid independence was demonstrated for higher Reynolds numbers. Up to $Re \approx 400$ the experimental and numerical results did not yield any additional regions of separaton apart from the primary one attached to the step. Good agreement between experiments and predictions is obtained under these conditions.

For a Reynolds number $Re = 389$, figure 16 shows, for the first sixteen x-stations, the measured U-velocity profiles and the corresponding predictions. At x-stations between 7 and 12 step heights downstream of the step, small deviations are indicated between the experimentally obtained velocity profiles and those deduced from two-dimensional numerical predictions. Although experimentally and numerically no additional region of separated flow is found on the channel side opposite to the step, the flow inside the experimental test rig showed small deviations from two-dimensionality. At higher Reynolds numbers at which multiple regions of separated flow are found experimentally and numerically, the experimental flow loses its two-dimensionality completely. This explains the discrepancies between experimental and numerical results indicated in figure 17.

In the published literature only a few velocity and/or reattachment length measurements exist for internal flow downstream of a single two-dimensional backward-facing step. The measurements reported by Abbot & Kline (1962) were obtained for turbulent flow and in a test-section geometry similar to the one employed in this study. Their measurements of reattachment length agree very well with the authors' data for high Reynolds number, where $x_R/S \approx 8$ was found for $Re \approx 6000$.

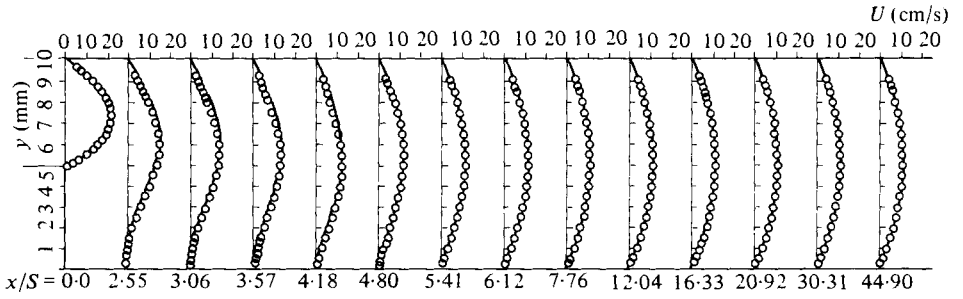

FIGURE 15. Experimental and theoretical velocity profiles for $Re = 100$ at different x/s-locations.

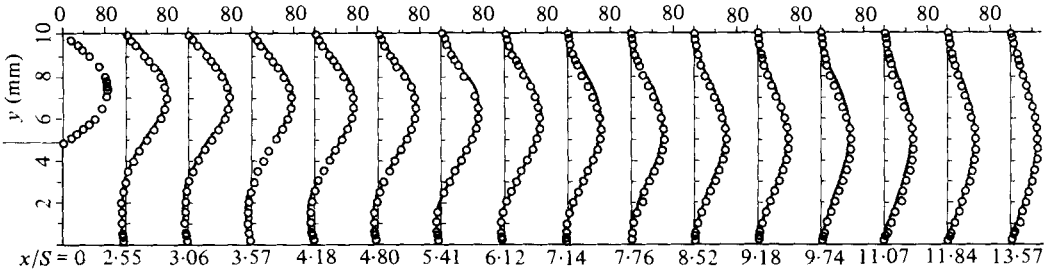

FIGURE 16. Experimental and theoretical velocity profiles for $Re = 389$ at different x/s-locations.

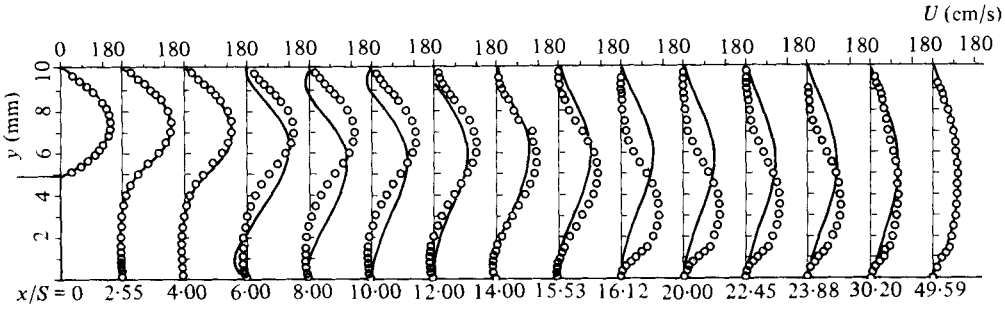

FIGURE 17. Experimental and theoretical velocity profiles for $Re = 1000$ at different x/S-locations.

All other reattachment lengths reported in the literature for turbulent backward-facing step flows were smaller than 8. Existing information suggests this to be due to differences in test-section geometries. A review of available results, provided by Durst & Tropea (1981), clearly indicates a decrease in reattachment length with decreasing expansion ratio $H/h = 1 + S/h$ at a constant Reynolds number.

In the laminar-flow region, measurements of detailed velocity distributions were carried out by Denham & Patrick (1974) and of reattachment length by Denham & Patrick and Goldstein *et al.* (1970). Figures 18(*a*, *b*) indicate that both sets of data compare well with the authors' separation-length measurements when plotted versus a Reynolds number defined on the diagrams. This would suggest that a Reynolds number based on the step height might be used as a single parameter that defines the reattachment length in a laminar two-dimensional backward-facing step flow.

This conclusion was examined by utilizing numerical solutions for reattachment

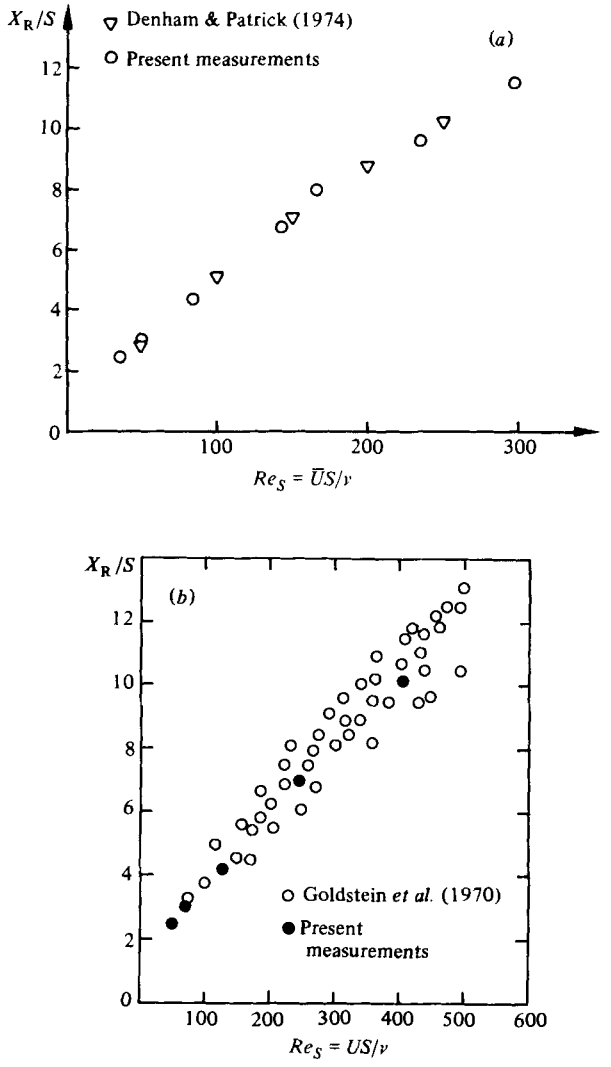

FIGURE 18. (*a*) Comparison with Denham & Patrick's (1974) results. (*b*) Comparison with the results of Goldstein *et al.* (1970).

length obtained by TEACH for laminar flows at $Re \lesssim 380$. The reattachment length for a fixed step Reynolds number in channels with different expansion ratios were computed, and it was shown that the conclusion drawn from figures 18(*a*, *b*) was incorrect. This indicates that the good agreement of the measured values shown in figures 18(*a*, *b*) is quite accidental. This confirms that the reattachment length in laminar two-dimensional backward-facing step flows is not a function of a single variable but is more likely to be a function of three or more variables, including the expansion ratio, the step or inlet-section Reynolds number and the slope at the wall of the inlet velocity profile.

Measurements in the laminar–turbulent transition region of a backward-facing step flow do not exist for comparison with the present values. In addition, computational schemes have not yet been developed for numerically treating this regime of the flow. It is clearly the more complex region for predictions or measurements because of the

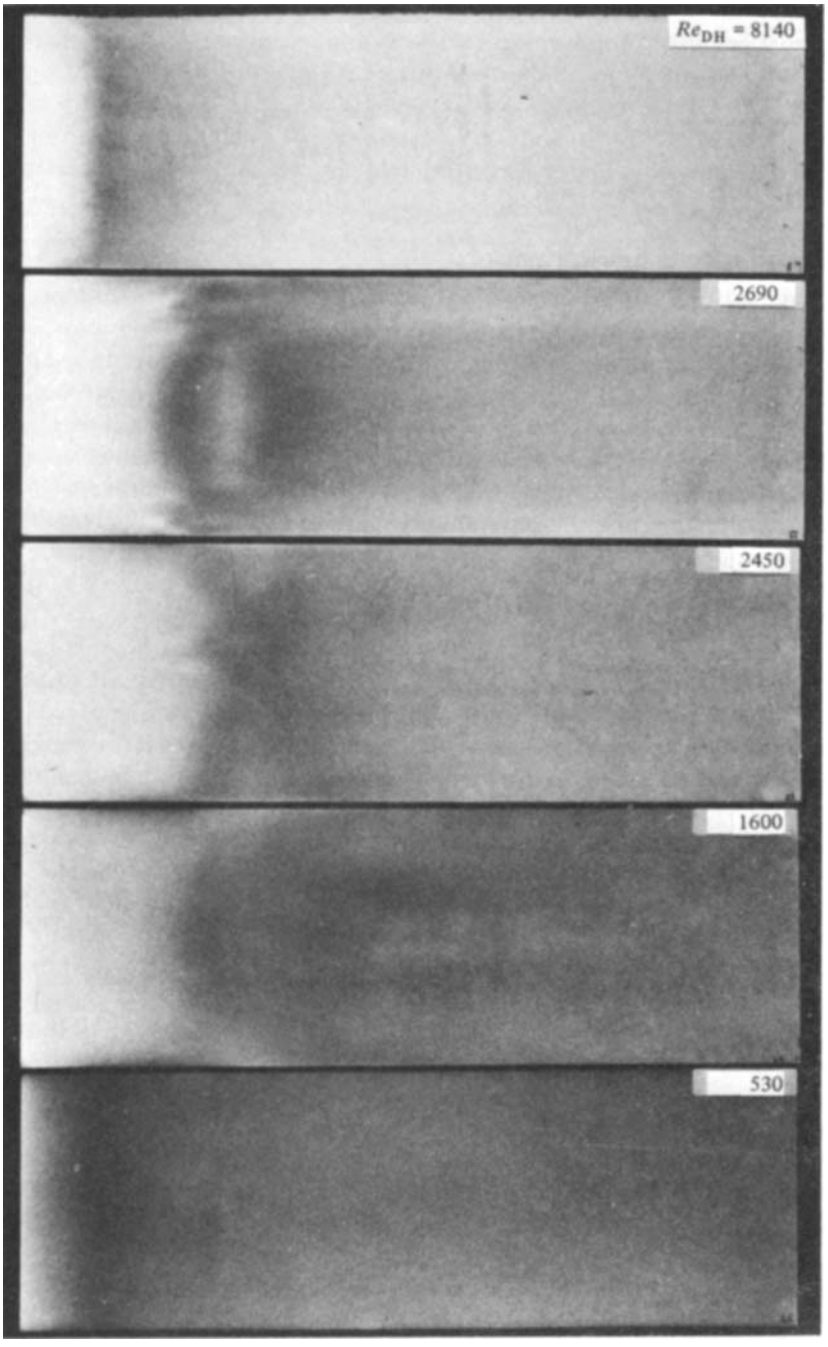

FIGURE 19. Mass-transfer measurements on the step-side wall, by Armaly *et al.* (1980).

presence of several recirculation regions that develop downstream of the step. Mass-transfer measurements, utilizing an ammonia-absorption scheme, described by Kottke *et al.* (1977), were performed in the same experimental channel and have been reported by Armaly *et al.* (1980). These mass-transfer measurements clearly show the second recirculation zone on the lower wall, as can be seen in figure 19. They also indicate clearly that within and around the transition regime longitudinal vortices

develop and destroy the two-dimensional character of the flow. Armaly *et al.* show that the vortices start to develop in the laminar region, $Re \approx 800$, become very pronounced at $Re = 2300$, and damped out at $Re = 5000$. It is interesting, however, to note that the mass-transfer measurements indicate clearly that in both the pure-laminar ($Re \lesssim 400$) and the fully turbulent ($Re \gtrsim 6600$) flow regimes, the flow is indeed two-dimensional over large parts of the width of the test section.

5. Conclusions and final remarks

Experimental investigations of laminar, transitional and turbulent flows with regions of separation behind a two-dimensional backward-facing step were carried out, and confirmed that laser-Doppler measurements can provide detailed information on the flow structure in the entire flow regime. Velocity profiles were obtained for various Reynolds numbers and at various x-stations downstream of the step. The length of the recirculating-flow region in the immediate vicinity of the backward-facing step was measured and its strong dependence on Reynolds number was quantified. In the laminar-flow regime the separation length increased with increasing Reynolds number, but not in the linear manner observed for axisymmetric sudden-expansion test sections. This increase occurred up to a Reynolds number of approximately $Re = 1200$. A further increase in Reynolds number caused the velocity fluctuations to increase, indicating the beginning of transition to turbulent flow. It is shown that transition from laminar to turbulent flow is characterized by an initially strong decrease in the main separation region attached to the step.

A recirculating-flow region was also observed on the test-section wall opposite to the step which initially increased and then decreased in size with increasing Reynolds number and decayed when the flow became fully turbulent. The axial dimensions of this additional recirculating-flow region are quantified in the paper together with the cross-sectional velocity profiles to provide a complete picture of the entire flow structure downstream of the two-dimensional step. The measurements show that the additional separation region on the wall opposite to the step changes its location in accordance with the location changes of the reattachment point of the primary region of separation.

The numerical predictions presented in this paper confirmed that available computer codes for flow predictions can be successfully employed to compute backward-facing step flows, with results in close agreement with experiments, at least up to Reynolds numbers of approximately 400. At this value, Reynolds number measurements and predictions start to deviate from each other. The deviations are explainable by the inherent three-dimensionality of the experimental flow for $Re \gtrsim 400$; it is present in the test section as soon as the second separation region exists on the wall opposite to the step.

A separation region on the wall opposite to the step was also predicted by the numerical scheme, and this additionally confirms that the strong adverse pressure gradient, due to the sudden cross-section change at the step, can cause the flow to separate also at the wall opposite to the step location. Two additional regions of recirculating flow were predicted on the channel wall where the step is located. Detailed information on some of the theoretical results obtained by the authors is provided. These confirm the strong dependence of the extensions of the region of separation on the cross-section ratio of the channels before and behind the step and also on the shape of the velocity profile at the point of separation. This information was used in order to explain differences among data available in the literature.

The present work was supported by the Deutsche Forschungsgemeinschaft within the framework of a research project on separated flows. The receipt of a Fulbright Fellowship by the first author and a DAAD Fellowship by the third author are gratefully acknowledged. Without these, the present work would have not been possible.

The paper benefited from useful discussions with Dr V. Kottke and Dr A. K. Rastogi. The help of Mr R. Gerber in constructing the test section is thankfully acknowledged. Miss Gaby Bartman was very helpful in preparing the final manuscript.

REFERENCES

ABBOTT, D. E. & KLINE, S. J. 1962 Experimental investigations of subsonic turbulent flow over single and double backward-facing steps. *Trans. A.S.M.E.* D: *J. Basic Engng* **84**, 317.

ARMALY, B. F., DURST, F. & KOTTKE, V. 1980 Momentum, heat and mass transfer in backward-facing step flows. *Sonderforschungsbereich* 80, *Universität Karlsruhe.*

BACK, L. H. & ROSCHKO, E. J. 1972 Shear layer flow regimes and wave instabilities and reattachment lengths downstream of an abrupt circular channel expansion. *Trans. A.S.M.E.* E: *J. Appl. Mech.* **39**, 677.

BREDERODE, V. DE & BRADSHAW, P. 1972 Three-dimensional flow in nominally two-dimensional separation bubbles. Flow behind a rearward-facing step. *I.C. Aero-Rep.* 72–19.

CASTRO, I. P. 1978 The numerical prediction of recirculating flows, *Proc. Int. Conf. on Numerical Methods in Laminar and Turbulent Flow, London.*

CHERDRON, W., DURST, F. & WHITELAW, J. H. 1978 Axisymmetric flows and instabilities in symmetric ducts with sudden expansions. *J. Fluid Mech.* **84**, 13.

DENHAM, M. K. & PATRICK, M. A. 1974 Laminar flow over a downstream-facing step in a two-dimensional flow channel. *Trans. Inst. Chem. Engrs* **52**, 361.

DURST, F. & TROPEA, C. 1977 Processing of laser-Doppler signals by means of a transient recorder and digital computer. *SFB* 80/E/118, *Sonderforschungsbereich* 80, *Universität Karlsruhe.*

DURST, F. & TROPEA, C. 1981 Turbulent, backward-facing step in two-dimensional ducts and channels. In: *Proc. Turbulent Shear Flow* 3 *Symp. Davis, September* 1981.

DURST, F. & WHITELAW, J. H. 1971 Aerodynamic properties of separated gas flows: existing measurements techniques and new optical geometry for the laser-Doppler anemometer. *Prog. Heat Mass Transfer* **4**, 311.

EATON, J. K. & JOHNSTONE, J. P. 1980 An evaluation of data for the backward-facing step flow. *Report prepared for* 1980/81 *Conference on Complex Turbulent Flows, Stanford University.*

ETHERIDGE, D. W. & KEMP, P. H. 1978 Measurements of turbulent flow downstream of a backward-facing step. *J. Fluid Mech.* **86**, 545.

FILETTI, W. G. & KAYS, W. W. 1967 Heat transfer in separated, reattachment and redevelopment regions behind a double step at the entrance to a flat duct. *Trans. A.S.M.E.* C: *J. Heat Transfer* **89**, 163.

GERSTEN, K. & WAUSCHKUHN, P. 1978 Über die abgelöste turbulente Strömung bei endlichem Ablösegebiet. *Bericht* No. 63/1978, *Lehrstuhl für Strömungsmechanik, Ruhr-Universität Bochum.*

GOLDSTEIN, R. J., ERIKSEN, V. L., OLSON, R. M. & ECKERT, E. R. G. 1970 Laminar separation reattachment, and transition of flow over a downstream-facing step. *Trans. A.S.M.E.* D: *J. Basic Engng* **92**, 732.

GOSMAN, A. D. & PUN, W. M. 1974 Lecture notes for course entitled: 'Calculation of recirculating flow'. *Heat Transfer Rep.* HTS/74/2, *Imperial College, London.*

KOTTKE, V., BLENKE, H. & SCHMIDT, K. G. 1977 Einfluß von Anströmprofil und Turbulenzintensität auf die Umströmung längsangeströmter Platten endlicher Dicke. *Wärme- und Stoffübertragung* **10**, 9.

KUMAR, A. & YAJNIK, K. S. 1980 Internal separated flows at large Reynolds number. *J. Fluid Mech.* **97**, 27.

LEONARD, B. P., LESCHZINER, M. A. & MCGUIRK, J. 1978 Third-order finite-difference method for steady two-dimensional convection. *Proc. Int. Conf. on Numerical Methods in Laminar and Turbulent Flow, London.*

LEONARD, P. B. 1979 A stable and accurate convective modelling procedure based in quadratic upstream interpolation. *Comp. Meth. in Appl. Mech. Engng* **19**.

LESCHZINER, M. A. 1980 Practical evaluation of three finite difference schemes for the computation of steady-state recirculating flows. *Comp. Meth. Appl. Mech. Engng* **23**, 293.

LESCHZINER, M. A. & RODI, W. 1981 Calculation of annular and twin parallel jets using various discretization schemes and turbulence-model variations. *Trans. A.S.M.E.* I: *J. Fluids Engng* **103**, 352.

MACAGNO, E. O. & HUNG, T. K. 1967 Computational and experimental study of a captive annular eddy. *J. Fluid Mech.* **28**, 43.

MOSS, W. D., BAKER, S. & BRADBURY, L. S. J. 1979 Measurements of mean velocity and Reynolds stresses in some regions of recirculating flows. In *Turbulent Shear Flows* 1 (ed. F. Durst, B. C. Launder, F. W. Schmidt & J. H. Whitelaw). Springer.

RAITHBY, G. D. 1976 Skewed upwind differencing schemes for problems involving fluid flow. *Comp. Meth. Appl. Mech. Engng* **19**, 153.

SEBAN, R. A. 1964 Heat transfer to the turbulent separated flows of air downstream of a step in the surface of a plate. *Trans. A.S.M.E.* C: *J. Heat Transfer* **86**, 259.

SPARROW, E. M. & KALJES, J. P. 1977 Local convective transfer coefficients in a channel downstream of a partially constructed inlet. *Int. J. Heat Mass Transfer* **20**, 1241.

VAHL DAVIS, G. DE & MALLINSON, G. D. 1976 An evaluation of upwind and central difference approximations by a study of recirculating flow. *Comp. Fluids* **4**, 29.

WAUSCHKUHN, P. & VASANTA RAM, V. 1975*a* Die turbulente Grenzschicht hinter einem Ablösegebiet. *Z. Flugwiss.* **23**, 1.

WAUSCHKUHN, P. & VASANTA RAM, V. 1975*b* Die turbulente Grenzschicht unmittelbar hinter dem Wiederanlegen eines Ablösegebietes. *Z. angew. Math. Mech.* **55**, T166.